Evolution of grain and subgrain structure during cold rolling of commercial-purity titanium

S.V. Zherebtsov[a], G.S. Dyakonov[a], A.A. Salem[b,c], S.P. Malysheva[d], G.A. Salishchev[a], S.L. Semiatin[b]

[a] Laboratory of Bulk Nanostructured Materials, Belgorod State University, Pobeda – 85, Belgorod, 308015, Russia
[b] Air Force Research Laboratory, Materials & Manufacturing Directorate, Wright-Patterson Air Force Base, Dayton, OH 45433-7817, USA
[c] Universal Technology Corporation, Dayton, OH 45432, USA
[d] Institute for Metals Superplasticity Problems RAS, Khalturin 39, Ufa, 450001, Russia

A B S T R A C T

The evolution of microstructure in commercial-purity titanium during cold rolling to a thickness strain of 2.6 was quantified using electron backscatter diffraction. The measurements were analyzed in terms of the mean grain size and the density of boundaries (the ratio of total boundary length to the scanned area). The density of high-angle boundaries as a function of thickness strain had three distinct stages, each of which was associated with a different mechanism of microstructure formation, i.e., (i) twinning, (ii) an increase in dislocation density and the formation of substructure, and (iii) the formation of deformation-induced high-angle boundaries. The influence of twinning on the kinetics of microstructure evolution was also interpreted.

Keywords:
Titanium
Cold rolling
Microstructure
Twinning
Grain refinement
EBSD

1. Introduction

Much attention has recently been given to the influence of large plastic deformation on microstructure evolution and the resulting properties of metals and alloys. This interest arises from the substantial refinement of microstructure during heavy cold working that leads to a considerable increase in strength and fatigue life and a decrease in superplastic-forming temperature [1,2]. Most of this work has focused on cubic metals using processes such as heavy cold rolling, multi-axis forging, and equal-channel angular extrusion [e.g., [3]].

The evolution of the microstructure in single-phase cubic metals during deformation comprising low-to-medium strains (von Mises strain $\varepsilon_{vM} \leq 0.8$) is generally associated with the formation of long microbands and dense dislocation walls surrounding groups of cells in cell blocks. After large strains ($\varepsilon_{vM} > 1$), lamellar high-angle, geometrically necessary boundaries parallel to the deformation direction, which delimit narrow slabs of cells or equiaxed subgrains formed by incidental dislocation boundaries, are developed [4].

Compared to cubic metals, the evolution of the microstructure during large deformation of hexagonal-closed pack (hcp) metals such as titanium has been investigated to a much less extent at cold working conditions. Unlike cubic metals with their large number of slip systems (e.g., twelve for fcc metals), hexagonal metals have far fewer deformation modes to accommodate arbitrary imposed strains in polycrystalline aggregates. For example, room temperature deformation of pure titanium may readily activate only four independent slip systems (two basal ⟨a⟩ and two prism ⟨a⟩ systems) [5]. To accommodate tensile or compression strains along the *c*-axis, either pyramidal ⟨c + a⟩ slip (with its associated higher critical resolved shear stress) or deformation twinning must be activated. The limited number of slip systems in hcp metals may result in the formation of unstable walls of edge dislocations rather than stable dislocation boundaries [6] such as high-angle deformation-induced boundaries. The objective of the present work, therefore, was to quantify the evolution of microstructure in terms of the grain size and the fraction of high-angle boundaries during cold rolling of commercial-purity titanium (CP Ti) to large thickness strains (ε_{th}).

2. Material and experimental procedures

A 4 mm thick slab of commercial-purity titanium (impurities in wt.% less than: 0.18 Fe, 0.1 Si, 0.07 C, 0.04 N, 0.01 H, 0.12 O was used in the present investigation. In the as-received condition, the slab had a homogeneous, equiaxed microstructure with an average grain size of 15 μm. All experiments were preformed on material in the as-received condition.

Table 1
Some parameters of EBSD analysis.

True thickness strain, ε_{th}	Scanned area (μm^2)	Scan step size (μm)	Average CI
0.05	139777.50	0.85	0.28
0.11	125798.4	0.75	0.35
0.16	112317.5	0.6	0.11
0.22	4493	0.09	0.2
0.36	79889.23	0.33	0.22
0.51	3664.5	0.08	0.11
0.92	7747.2	0.1	0.13
2.66	1732.542	0.05	0.09

To determine the effect of the degree of deformation on microstructure evolution, rectangular samples were rolled at room temperature using a fixed rolling speed of 30 mm/s. Unidirectional multipass rolling was carried out using ~5 pct. reduction per pass. Samples were extracted from the rolled sheet after total reductions of 5, 10, 15, 20, 30, 40, 60 and 93 pct., corresponding to true thickness (compressive) strains ε_{th} of 0.05, 0.1, 0.16, 0.22, 0.36, 0.51, 0.92, and 2.66, respectively.

Microstructure and crystallographic texture at the mid-thickness rolling plane of each sample were determined using light microscopy, transmission electron microscopy (TEM), and electron-backscatter-diffraction (EBSD) technique. TEM was done in a JEOL JEM-2100FX. The dislocation density was measured by counting the individual dislocations in grain/subgrain interiors on at least six arbitrarily selected typical TEM images for each sample. EBSD was conducted in a Quanta 600 field-emission-gun scanning-electron microscope (FEG SEM) equipped with a TSL OIM^{TM} system version 5.2. Some parameters of EBSD analysis are shown in Table 1. A boundary misorientation of 15° was used to define high-angle boundaries. In the EBSD inverse-pole-figure maps presented below, gray and black lines indicate low-angle boundaries (LABs) and high-angle boundaries (HABs), respectively. Due to the experimental error in evaluating orientations by EBSD [7], grain-boundary misorientations below 2° were excluded from the data analysis.

Each non-indexed data point was automatically re-assigned to the crystallographic orientation of its nearest neighbor in order to obtain a high fidelity picture of the microstructure. However EBSD maps of heavily deformed titanium may contain a lot of unsolved pixels. For example, approximately 70 pct. of unsolved pixels after 90 pct. cold rolling was reported in [8]. To improve the quality of EBSD data, the specimen cold rolled to $\varepsilon_{th} = 2.66$ was annealed at 350 °C for 1 h. This temperature was lower than the expected static recrystallization temperature by ~50 °C (judging by the change in microhardness with temperature (Fig. 1). The average confidential index (CI) of the EBSD analysis was improved to a more or less

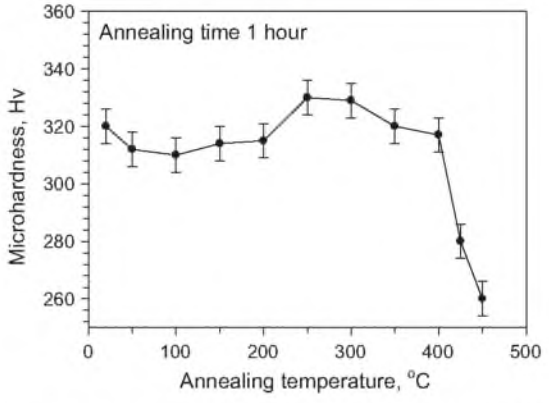

Fig. 1. Effect of annealing temperature on the microhardness of CP Ti cold rolled to thickness strain $\varepsilon_{th} = 2.66$. Annealing time was 1 h.

acceptable value of 0.09 (Table 1). Changes in the microstructure caused by annealing are discussed in subsequent sections.

The density of boundaries ρ_b was calculated as the ratio of the total length of boundaries (either low-angle or high-angle) to the area of the scan. During quantitative analysis edge grains and unindexed points were omitted from consideration.

3. Results and discussion

Rolling-plane normal-direction (ND) inverse-pole-figure (IPF) maps for CP Ti in the as-received condition and cold rolled to thickness reduction $\varepsilon_{th} = 0.1, 0.36, 0.92$ and 2.66 are shown in Fig. 2; the last map was obtained from the specimen additionally annealed at 350 °C for 1 h. In the as-received condition, the microstructure consisted of equiaxed grains with an average size of 15 μm (Fig. 2a). The grains contained no twins and essentially no internal substructure. After $\varepsilon_{th} = 0.1–0.36$, a large number of twins were observed within the majority of the grains; however some grains contained no twins even after a strain $\varepsilon_{th} = 0.36$ (Fig. 2b and c). A pronounced difference between the microstructures after $\varepsilon_{th} = 0.1$ and $\varepsilon_{th} = 0.36$ was revealed by the development of substructure in the latter case. Cold rolling to a thickness strain of 0.92 increased the number of small equiaxed grains considerably and resulted in the formation of dense substructure within large grains (Fig. 2d and e). The heaviest thickness reduction ($\varepsilon_{th} = 2.66$) gave rise to a microstructure consisting of a mixture of small equiaxed grains and large grains containing many sub-boundaries (Fig. 2f and g).

TEM observations showed that cold rolling to a thickness strain $\varepsilon_{th} = 0.92$ gave rise to a cellular microstructure with a high dislocation density (Fig. 3a). Cell boundaries were rather wide and loose. The size of the cells varied over a wide range from a hundred nanometers to a few micrometers. Separate (sub)grains with a size of 100–200 nm and thin clear boundaries were also observed in the structure. The dislocation density within such grains was lower than that in the matrix.

Cold rolling to $\varepsilon_{th} = 2.66$ led to a considerable refinement of the microstructure and simultaneously to an increase in dislocation density (Fig. 3b). The size of cells was found to be approximately 200 nm. Small subgrains (~100 nm) were also seen in the background of the cell structure. Annealing of the specimen cold rolled to $\varepsilon_{th} = 2.66$ resulted in a noticeable decrease in dislocation density (by a factor of 1.3), a thickening of cell boundaries, and an increase in the number of globular, almost dislocation-free subgrains (Fig. 3c). The size of new subgrains was found to be ~100–200 nm. Consequently, such changes in microstructure appeared to correspond to well-developed recovery and the beginning of recrystallization. The TEM microstructure observations impacted the quantitative results of EBSD analysis by increasing the total length and fraction of HABs. However the fraction of new small grains or subgrains was rather small and their contribution to the length of HABs and LABs was expected to be small.

Quantitative data derived from the EBSD analysis revealed an increase in the fraction of LABs to 0.66 with an increase in thickness strain to $\varepsilon_{th} = 0.51$ (Fig. 4). However, with further cold rolling to $\varepsilon_{th} = 2.66$, the fraction of LABs decreased to 0.57. An analysis of the misorientation distributions (Fig. 5) suggested that the initial increase in the fraction of LABs was mainly associated with an increase in the number of boundaries with intermediate low-angle misorientation (Fig. 5 c, e and g). It is also worth noting that in the strain interval between 0.1 and 0.92, the fraction of those boundaries which had low-to-medium misorientation was very low. However, the misorientation bin with the fewest boundaries shifted to higher angles with thickness strain. Specifically, there were almost no boundaries with misorientations of ~10° at $\varepsilon_{th} = 0.1$, while boundaries with a misorientation of 20° were scarce

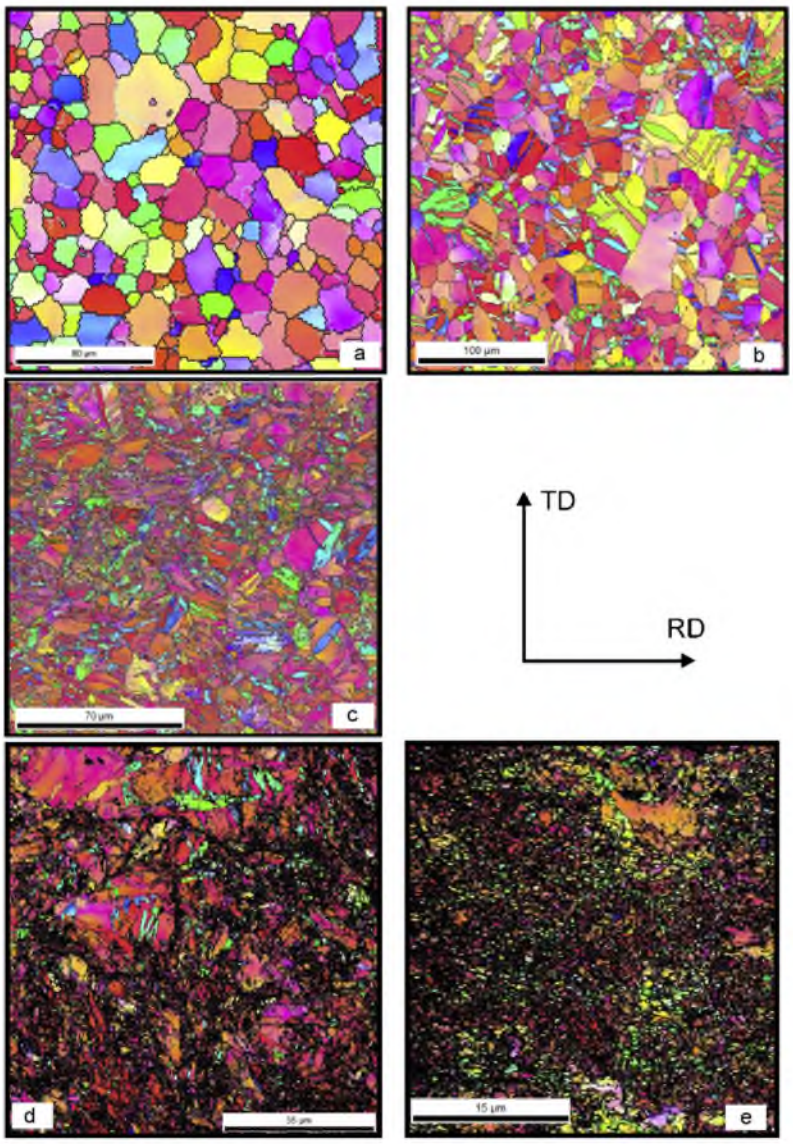

Fig. 2. Normal-direction EBSD (inverse-pole-figure) maps taken on the mid-thickness rolling plane of titanium samples cold rolled to thickness strain ε_{th} of (a) 0, (b) 0.1, (c) 0.36, (d) 0.92, or (e) 2.66. EBSD maps of highly-deformed material (ε_{th} = 0.92 and 2.66) are shown in the as-scanned conditions for points with CI > 0.1 (d and e). The map corresponding to ε_{th} = 2.66 (e) was obtained after annealing at 350 °C for 1 h.

after 0.36 and 0.92 thickness strain (Fig. 5). Both the trend in the evolution of the misorientation distributions and the change in the fraction of LABs (and the corresponding behavior of the HABs) is typical for various metallic materials [9,10] and can be attributed to the gradual increase in cell/subgrain misorientation and the more rapid decrease in HAB spacing than the subgrain size with thickness strain, respectively.

The high-angle boundaries exhibited two peaks corresponding to 65° and 85° following ε_{th} of 0.1–0.36 (Fig. 5c and e). Mirroring the microstructure observations in the inverse-pole-figure maps (Fig. 2b and c), these peaks can be associated with formation of 65.62° $\langle 10\bar{1}0\rangle$ and 84.78° $\langle 2\bar{1}\bar{1}0\rangle$ boundaries corresponding to $\{11\bar{2}2\}\langle 11\bar{2}\bar{3}\rangle$ and $\{10\bar{1}2\}\langle\bar{1}011\rangle$ twins, respectively. In previous work, Chun et al. [8] reported the formation the same twin families in cold-rolled CP Ti in the ε_{th} interval of 0.1–0.5.

The evolution of the overall texture was typical for the cold rolling of CP Ti [e.g., [8]]. In the as-received condition, the (0 0 0 2) pole figure consisted primarily of a split texture with basal poles tilted ~30° from the ND toward the TD (Fig. 3b); weaker components were located approximately 80–90° from the ND toward the TD. In the $(10\bar{1}0)$ pole figure, the maximum intensity was located at the RD. Such pole figures are typical for hot-rolled titanium sheet products [11]. Texture evolution during cold rolling to ε_{th} = 0.1–0.36 was associated with some weakening of basal poles and the appearance of new weak peaks due to twinning (Fig. 5d and f). By 0.92 thickness strain, the influence of twinning on texture evolution almost saturated, and the texture (Fig. 5h) had started to become similar to that observed in the initial condition. Likewise, pole figures after ε_{th} = 2.66 reduction were very similar to that observed in the initial condition (Fig. 5j). However the texture components after heavy cold rolling were sharper and had higher intensity.

Although it is convenient to discuss microstructure evolution in terms of the fraction of HABs, it should be recognized that such an approach is rather approximate. Additional quantitative insight was obtained from an analysis of the density of LABs and HABs (calculated from the EBSD data) as a function of thickness strain (Fig. 6a). These results suggested three distinct stages in the formation of HABs during cold rolling while only two stages were observed for LABs.

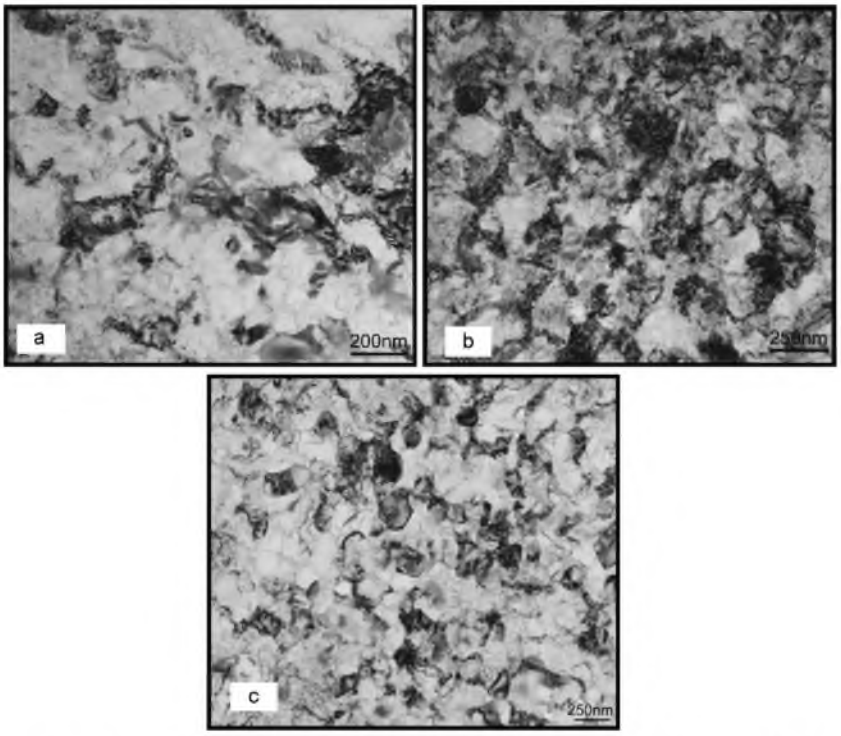

Fig. 3. Transmission-electron micrographs of cold rolled CP-Ti: (a) $\varepsilon_{th} = 0.92$ (as-rolled); (b) $\varepsilon_{th} = 2.66$ (as-rolled), and (c) $\varepsilon_{th} = 2.66$ (rolled and then annealed 1 h at 350 °C).

The first stage in the formation of HABs (ε_{th} between 0 and ~0.2) can be associated with marked twinning as observed in Figs. 2b and c and 5c and e. Twinning also influences the dislocation structure developed during deformation. The interaction between dislocations and twins in hcp metals gives rise to dislocation pile-ups at the twin-matrix interfaces and local stress concentrations [12]. Such an effect leads to Hall-Petch hardening due to a reduction in the effective slip distance by twin boundaries which act as barriers to slip [13]. Another hardening factor, proposed by Basinski et al. [14] and experimentally demonstrated by Salem et al. [15], arises from the transition of dislocations from glissile to sessile configurations within the twins, thereby contributing to the formation of low-angle dislocation walls within the microstructure (Fig. 5c and e). Because twin formation and the Basinski effect are closely interrelated, it is not surprising that the rate of increase of the densities of HABs and LABs were almost equal to each other at low levels of deformation.

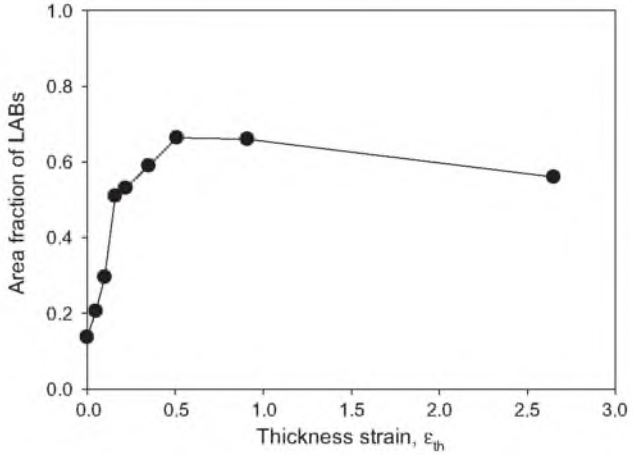

Fig. 4. Area fraction of LABs in cold-rolled CP Ti as a function of thickness strain.

It should be noted that during twinning, the factors that lead to strengthening (the Hall-Petch effect and the Basinski mechanism) may compete with texture softening due to lattice reorientation of the twinned regions, thereby resulting in a decreased rate of strain hardening [15]. In addition, because twinning accommodates a finite fraction of the imposed strain, the amount of required slip in the matrix (and hence the dislocation activity that controls microstructure refinement) is decreased relative to that necessary in the absence of twinning. Thus, microstructure refinement due to the formation of deformation-induced HABs may be shifted to larger strains as a result of twinning. In agreement with previous observations [8,13,15], twinning in the present work was found to saturate at a ε_{th} of ~0.2.

At higher ε_{th}, i.e., $0.2 \leq \varepsilon \leq 0.51$, the rate of increase in LAB density did not change (Fig. 6a). By contrast, a second stage of HAB formation at a rate noticeably lower than that in the first stage was observed. During this stage, the boundaries associated with the twin-matrix interfaces evolved with continued straining into arbitrary HABs as a result of twin/dislocation interactions [16]. In addition, dislocation substructure evolved as a result of classical dynamic recovery during which dislocation multiplication was mitigated by dislocation annihilation and the formation of sub-boundaries [15]. Consequently, after the exhaustion of twinning, the rate of increase of the dislocation density with strain might be expected to be close to that in the material which deforms by dislocation glide alone but at higher initial dislocation density. Nevertheless, a necessary condition for the formation of deformation-induced HABs appears to be a high level of stress at boundaries between areas having different slip systems [15] and/or the activation of multiple slip systems [17]. That is to say, deformation inhomogeneity promotes the formation of HABs. A decrease in effective grain size, such as that due to twinning, typically results in more homogeneous plastic flow [18] and thereby should shift the formation of deformation-induced HABs to larger strains. In this regard, the rate of microstructure refinement with strain has been found to be lower in an aluminum alloy with an initial fine grain microstructure relative to that in the same material with a

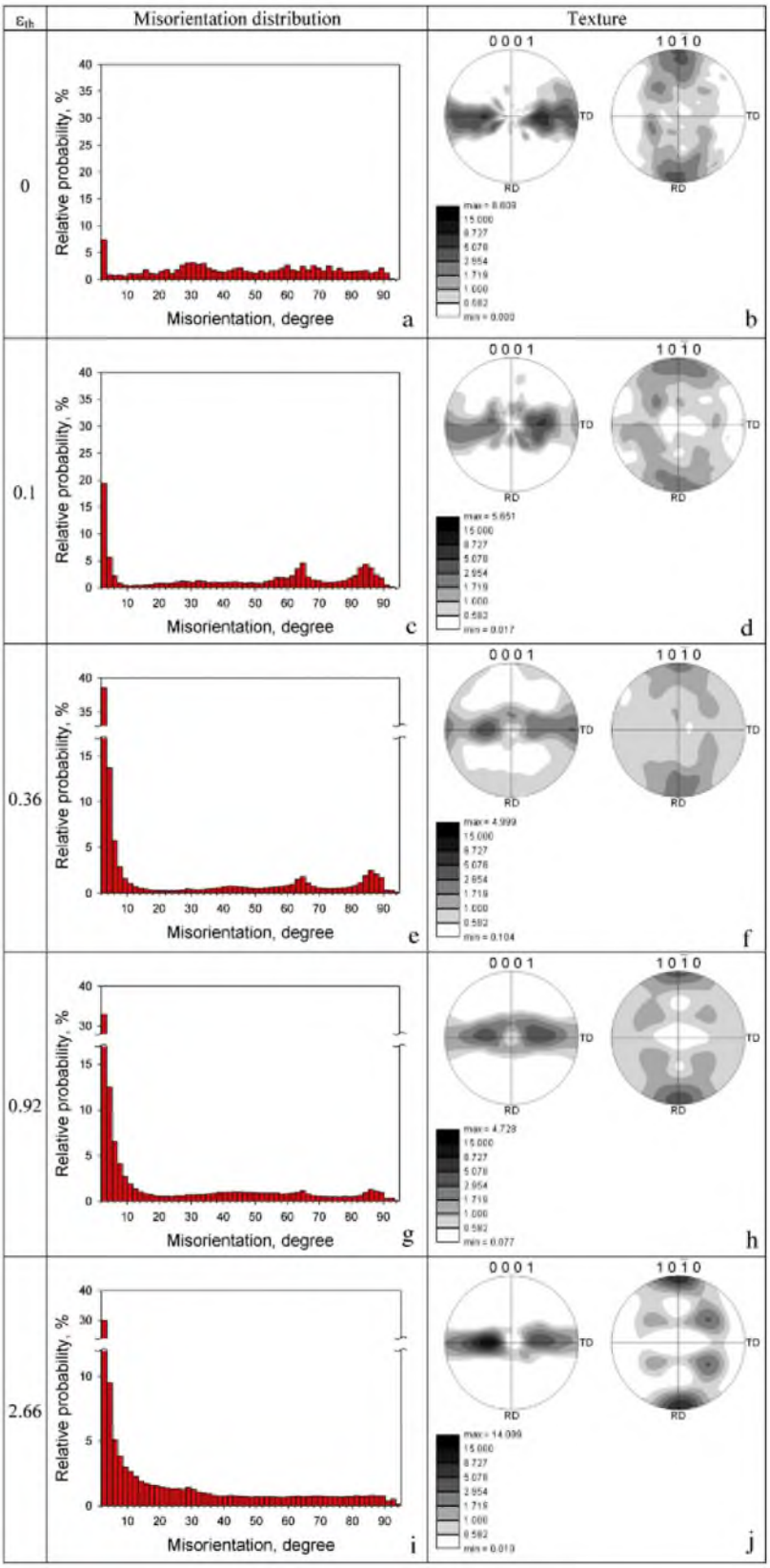

Fig. 5. Misorientation distributions (a, c, e, g and i) and (0 0 0 2) and (10$\bar{1}$0) pole figures (b, d, f, h and j) of CP Ti cold rolled to true thickness strains of 0, 0.1, 0.36, 0.92, and 2.66.

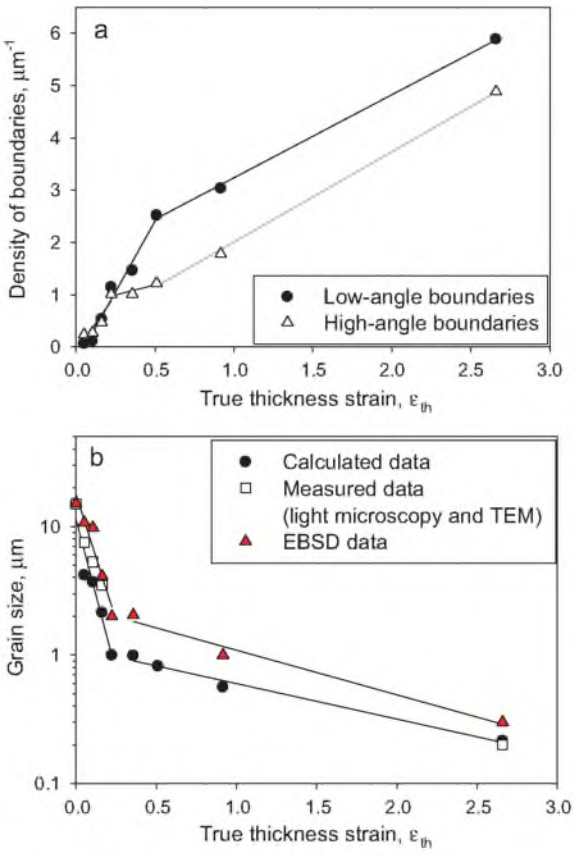

Fig. 6. Dependence on thickness strain of (a) the density of low- and high-angle boundaries and (b) grain size. Grain size was measured by optical microscopy and TEM after low and high strain respectively.

coarse starting microstructure [19]. For ε_{th} between approximately 0.2 and 0.5, therefore, the density of high-angle boundaries in CP Ti changed slowly, and the majority of microstructure evolution was associated with the formation of substructure within initial grains and twins (Figs. 2c and 5e). Thus, the second stage may be viewed in effect as an incubation period for the accumulation of a sufficient level of dislocation density for the subsequent formation of HABs.

The third, and final, stage in microstructure evolution (Fig. 6a) occurred at ε_{th} above ~0.5 and was most probably associated with the formation of high-angle deformation-induced boundaries [4] while the rate of LABs formation decreased measurably.

Although the density of LABs was found to be equal to or greater than that of HABs at all strain levels, the rate of increase of the density of LABs at strains above ~0.5 was lower than that of HABs, thus suggesting a decrease in the fraction of LABs as was observed (Fig. 4). This observation thus indicates the competition between the formation of LABs and the concurrent increase in LAB misorientations to high angles [8,20,21]. In the interval of ε_{th} between 0.5 and 0.9, the two processes balance each other (Fig. 4). According to literature data, the size of cells/subgrains tends to saturate at ε_{th} above approximately 1–1.5 [22]. Assuming that the new small grains essentially originate from the stain-induced subgrains, the subboundaries transform into grain boundaries and the size of the grains in heavily deformed materials approach that of these subgrains [e.g. [22]], thereby resulting in a decreased rate of LAB formation (Figs. 4 and 6a).

The internal consistency of the present results was demonstrated by comparing the measured grain size as a function of imposed thickness strain with that calculated from the HABs density, i.e., $d = 1/\rho_b$. The result (Fig. 6b) showed reasonable agreement between the calculations and grain-size measurements based on EBSD as well as optical and TEM micrographs. It should be noted that the coincidence of the grain size calculated from the EBSD data and obtained by TEM in the heavily deformed condition ($\varepsilon_{th} = 2.66$, Fig. 6b) implies indeed very small changes in the length of HABs after annealing at 350 °C for 1 h.

The semi-logarithmic plot in Fig. 6b also revealed distinct stages corresponding to (i) the twinning regime and (ii) the formation of deformation-induced HABs. Twinning resulted in rapid microstructure refinement but saturated at a grain size of only ~1–2 μm. Refinement of the microstructure to grain sizes of the order of 0.2 μm with further deformation was noted to occur much more slowly. It should be noted that the incubation (second) period in the grain size–thickness strain plot (Fig. 6b) was quite small and can hardly be separated as a stage. In particular, a close examination of the plot just after the completion of twinning revealed that the mean grain size did not change with strain for both the calculated and the EBSD plots. This result may indicate a lower sensitivity of grain size per se to thickness strain in comparison to boundary density.

4. Summary and conclusions

EBSD analysis of cold-rolled titanium revealed three stages of microstructure evolution. The first is associated with twinning. Being one of the main modes of deformation, twinning refines the microstructure but shifts the formation of high-angle deformation-induced boundaries and the accompanying grain refinement to larger strains. The final stage follows an intermediate, so-called incubation, strain interval. The three stages of microstructure evolution are well defined by plots of the density of high-angle boundaries as a function of thickness strain.

Acknowledgment

This work was supported by the Federal Agency for Education, Russia; Grant #P2486.

References

[1] M.A. Meyers, A. Mishra, D.J. Benson, Prog. Mater. Sci. 51 (2006) 427–556.
[2] K.S. Kumar, H. Van Swygenhoven, S. Suresh, Acta Mater. 51 (2003) 5743–5774.
[3] R.Z. Valiev, Yu. Estrin, Z. Horita, T.G. Langdon, M.J. Zehetbauer, Y.T. Zhu, JOM (2006) 33–39.
[4] D.A. Hughes, N. Hansen, Acta Mater. 48 (2000) 2985–3004.
[5] C. Leyens, M. Peters (Eds.), Titanium and Titanium Alloys: Fundamentals and Applications, Wiley-VCH Verlag GmbH, Weinheim, 2003.
[6] S. Mironov, M. Murzinova, S. Zherebtsov, G.A. Salishchev, S.L. Semiatin, Acta Mater. 57 (2009) 2470–2481.
[7] F.J. Humphreys, J. Microsc. 195 (1999) 170–185.
[8] Y.B. Chun, S.H. Yu, S.L. Semiatin, S.K. Hwang, Mater. Sci. Eng. A398 (2005) 209–219.
[9] F. Humphreys, M. Hatherly, Recrystallization and Related Annealing Phenomena, Elsevier, Oxford, 2004.
[10] G. Langford, M. Cohen, Metall. Trans. A6 (1975) 901–910.
[11] U. Zwicker, Titanium and Titanium Alloys, Springer-Verlag, Berlin, 1974.
[12] M.H. Yoo, Metall. Trans. 12A (1981) 409–418.
[13] A.A. Salem, S.R. Kalidindi, R.D. Doherty, Acta Mater. 51 (2003) 4225–4237.
[14] Z.S. Basinski, M.S. Szczerba, M. Niewczas, J.D. Embury, S.J. Basinski, Rev. Metall. 94 (1997) 1037–1043.
[15] A.A. Salem, S.R. Kalidindi, R.D. Doherty, S.L. Semiatin, Metall. Mater. Trans. A37 (2006) 259–268.
[16] G. Salishchev, S. Mironov, S. Zherebtsov, A. Belyakov, Mater. Charact. 61 (2010) 732–739.
[17] A.A. Salem, Z. Horita, T.G. Langdon, T.R. McNelley, S.L. Semiatin, Metall. Mater. Trans. A37 (2006) 2879–2891.
[18] M.A. Meyers, K.K. Chawa, Mechanical Behavior of Materials, Cambridge University Press, New York, 2009.
[19] H. Jazaeri, F.J. Humphreys, Acta Mater. 52 (2004) 3239–3250.
[20] W. Pantleon, Scr. Mater. 53 (2005) 757–762.
[21] J. Gil Sevillano, P. van Houtte, E. Aernoudt, Prog. Mater. Sci. 25 (1981) 69–412.
[22] N. Dudova, A. Belyakov, T. Sakai, R. Kaibyshev, Acta Mater. 58 (2010) 3624–3632.